Astron. Astrophys. 314, 615–624 (1996)

ASTRONOMY AND ASTROPHYSICS

Maps of the 36 GHz methanol emission*

S. Liechti[1] **and T.L. Wilson**[2]

[1] Centro Astronómico de Yebes (OAN-IGN), Apartado 148, E-19080 Guadalajara, Spain
[2] Max-Planck Institut für Radioastronomie, Auf dem Hügel, 69, D-53121 Bonn, Germany

Received 18 December 1995 / Accepted 7 February 1996

Abstract. We have used the Effelsberg 100-meter telescope to map the 36 GHz $4_{-1} \rightarrow 3_0$E methanol transition in galactic star forming regions where methanol masers were previously detected. In most sources, the emission consists in one or several narrow (maser) features superimposed on a broader, presumably quasi-thermal component. The line shapes and positions of the narrow features are often similar to those observed in the other Class I methanol maser transitions (at 25, 44, 84 and 95 GHz), but with some exceptions. Our observations confirm that, unlike the strong Class II methanol masers (at 12.2, and 6.6 GHz), the Class I methanol masers are offset from the compact H II regions, infrared sources and OH/H_2O masers. In outflow sources, these are located at the edge of the molecular lobes.

Key words: ISM: molecules – ISM: clouds – ISM: H II regions – radio lines: ISM

1. Introduction

The 36 GHz methanol masers are thought to belong to the Class I category. These are found in massive star forming regions, but are generally offset from ultra-compact H II regions and strong infrared sources, which mark the location of the newly formed stars (see e.g. Menten 1991a). The 36 GHz methanol transition ($4_{-1} \rightarrow 3_0$E) was first detected in the Sgr B2 star forming region, where some features are very intense ($\sim$ 200 K) with several narrow features ($\simeq$ 1 kms^{-1}) atop a broader pedestal ($\simeq$ 10 to 20 kms^{-1}). There is also a strong variation of intensity with position (Morimoto et al. 1985). In a limited survey, Haschick & Baan (1989) detected this transition toward 26 galactic H II regions. Six of these regions showed narrow spike emission suggesting maser emission. More complete surveys were carried out in the 44 GHz line and led to maser detections in more galactic H II regions (Haschick et al. 1990; Bachiller et al. 1990). However, the sensitivity, spatial and spectral resolution of these surveys were limited, precluding precise determinations of the maser positions. The aim of this survey was to use the unsurpassed sensitivity and resolution of the Effelsberg 100-m telescope at 36 GHz to map the regions where emission was detected in the previous surveys. The determination of the masers location is a necessary step for further interferometric observations. Priority was given to the sources where narrow spike emission was detected. Some sources reported as non-detections were also reobserved.

2. Observations

The observations were made with the Effelsberg 100-m telescope equipped with an HEMT amplifier. The half power beam width at 36.169 GHz is $\sim$ 26″. The facility 1024 channel autocorrelator was used with 6.25 MHz bandwidth, which corresponds to a resolution of $\sim$ 0.05 kms^{-1} at the line frequency. The total velocity coverage was 52 kms^{-1}. To obtain a better signal-to-noise ratio, the spectra were usually smoothed to $\sim$ 0.1 kms^{-1} resolution (or to $\sim$ 0.2 kms^{-1} for the very weak emission or tentative detections).

The observations were performed in 2 sessions, in October 1992 and in March 1993. In the second session, the observing time was divided between 5 (non consecutive) nights. Although the pointing was repeatedly checked during each observing session, maps reobserved in different sessions show that the pointing differences (as determined from the positions of the maser features in the maps) can be up to $\sim$ 15″, especially when the pointing source was $>$ 20° from the observed sources. These errors were caused by an incomplete set of parameters in the telescope pointing model. These differences appeared mainly between the October and March observing sessions. So depending on the source, the maximum absolute pointing errors are estimated to be between 5 and 10″; relative errors of features within a map are much smaller. For more details, see the discussion on individual sources below. Raster scanned maps (consisting of at least 3 × 3 points) were usually performed with 30 seconds integration time per position and 12 or 15″ spacings (depending on the sources). For some sources, observations obtained in different sessions were summed to obtain up to 90 seconds of integration time per position.

Send offprint requests to: T.L. Wilson

* Tables 1 to 4 and Figures 1, 3, 5 and 7 to 11 are only available in electronic form at the CDS via anonymous ftp 130.79.128.5.

For a few sources, complementary observations were performed in February 1994, with the autocorrelator split into 2 spectrometers of 512 channels each, centered at the same frequency (velocity resolution of $\sim 0.1\,\mathrm{kms}^{-1}$). For these observations, the on source integration time was 30 or 60 seconds per position and the spacings 10 or 20″, depending on the source.

The line intensities were calibrated using observations of strong continuum sources of known flux densities. For most sources, NGC 7027 was used, taking a flux density of 6 Jy. For the sources near the galactic center, the peak of Sgr B2(M) was used assuming a flux density of 15 Jy or equivalently a main beam brightness temperature of 21.6 K (Martin-Pintado et al. 1990).

3. Results

Of the 48 galactic sources observed, emission has been definitely detected in 34 sources and tentatively detected in 7 more (Tables 1 and 2). Among these, 28 sources show narrow ($\leq 1\mathrm{kms}^{-1}$) features; these are often superimposed on wider pedestals. This suggests that maser emission produces the narrow features (see discussion below). The number of masers is much larger than in the previous survey of Haschick & Baan (1989). In 24 sources, the emission is sufficiently strong to determine the peak position of the maximum and the source size (see Table 1). In the following, we discuss the most interesting sources.

3.1. Sgr B2

We have completely mapped the emission in the Sgr B2 region (Main and North), with 15″ spacing. Morimoto et al. (1985) first detected the 36 GHz methanol transition in this region. As with those data, the observed lines show a blend of very strong (up to 200 Jy) broad ($> 3\,\mathrm{kms}^{-1}$) features with a superposition of narrower ($\leq 1\,\mathrm{kms}^{-1}$) features (the underlying extended emission cannot be easily separated from the broader strong components). Our more extended map and better spatial resolution allow us to see many more components: more than 50 narrow ($\leq 1.5\,\mathrm{kms}^{-1}$) components, some $\leq 0.3\,\mathrm{kms}^{-1}$, and more than 12 broader components ($\geq 2.5\,\mathrm{kms}^{-1}$) can be distinguished (see Table 3 for the strongest of them). Most of these components appear point-like in our beam; those which seem extended might be several blended features. In fact, they appear more like a double-peaked structure than as smooth extended emission. Only the $6.8\,\mathrm{kms}^{-1}$ wide feature at $73.0\,\mathrm{kms}^{-1}$ appears to be clearly extended (about 30″ × 50″), and cannot be easily separated in several features. However, this could also be a blend of several narrower features. One should note that some features have clearly non-gaussian line shapes; see e.g. the features at $51\,\mathrm{kms}^{-1}$ at the position (−15″,135″) and the one at $58\,\mathrm{kms}^{-1}$ at the position (0″, 60″) (Fig. 1). As shown in Fig. 2, the strongest emission is found in a region about 90″ north of the main compact H II region (which was not observed by Morimoto et al. 1985), and the emission is distributed in a shell-like structure northwest of the compact H II regions. The overall distribution is strikingly similar to the HNCO, HC_3N and 1.3mm continuum emission distribution (Lis & Goldsmith, 1991). This distribution is anticorrelated with the $C^{18}O$(J=1–0) emission distribution.

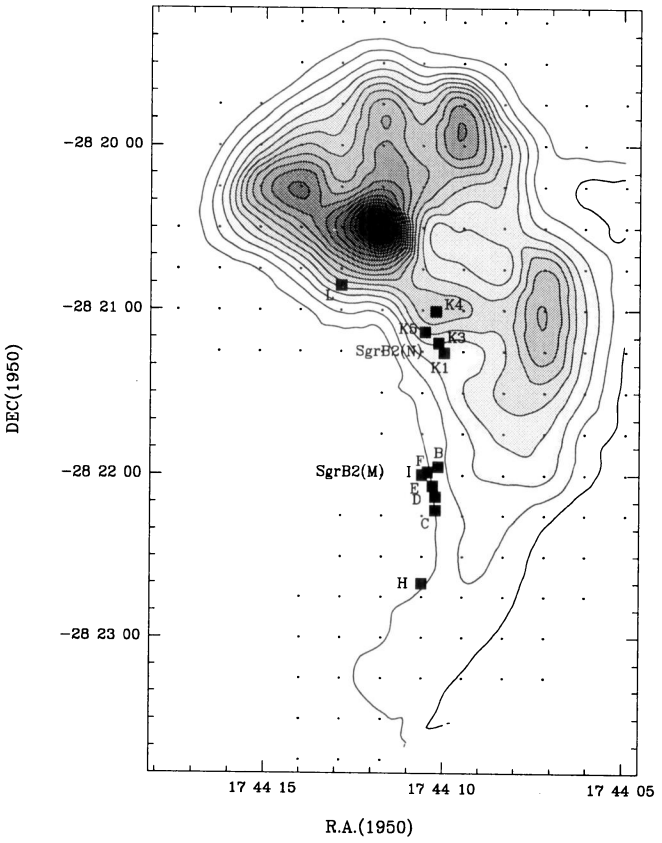

Fig. 2. Contour map of the 36 GHz methanol integrated intensity in Sgr B2 over the 42–88 km s^{-1} velocity range. The levels are from 200 to 2000 in steps of 100 Jy.kms^{-1}. The points are the observed positions, and the filled squares, the compact HII regions (positions from Gaume and Claussen 1990).

3.2. Sgr A

We observed the 36 GHz methanol transition in three regions close to the Galactic Center with 12 and 15″ spacings, and we have completely mapped the regions around Sgr A-A and Sgr A-F where strong emission was found; the most intense peak emission of our entire survey, nearly 300 Jy, was detected around the Sgr A-A position (Fig. 3). Sgr A-A is the most northern of several compact H II regions (A to D) located on the eastern edge of Sgr A East shell in the so-called "$50\,\mathrm{kms}^{-1}$" molecular cloud M−0.02 − 0.07, while Sgr A-F is a non-thermal continuum source on the southern edge of this shell and in the northern part of the "$20\,\mathrm{kms}^{-1}$" molecular cloud M−0.13 − 0.08 (Sgr A-G is located further south). In the Sgr A-A and Sgr A-F regions, the emission characteristics are very similar to that found in Sgr B2, that is, a blend of many strong broad and narrow features (Fig. 3 and Table 4), with the narrower ($< 3\,\mathrm{kms}^{-1}$) features point-like

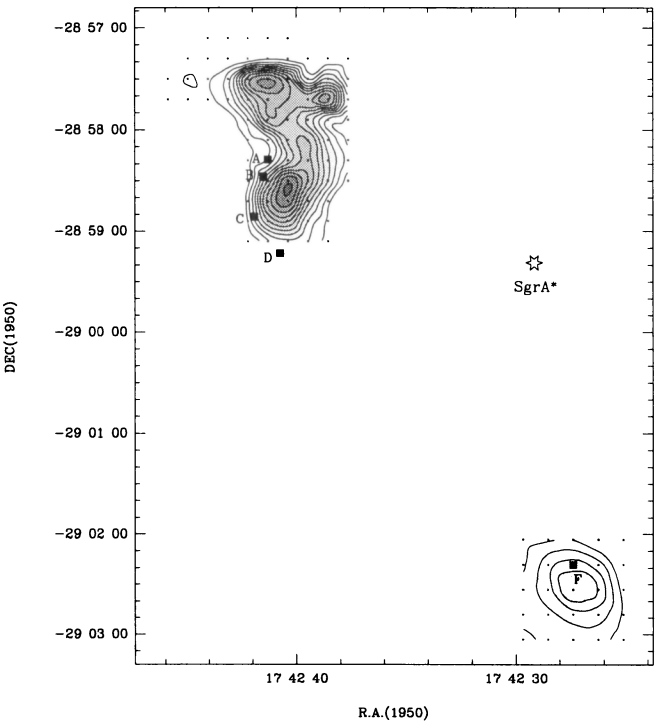

Fig. 4. Contour map of the 36 GHz methanol integrated intensity in Sgr A over the 20–67 km s^{-1} velocity range for the region around Sgr A-A and over the 0–40 km s^{-1} velocity range for the region around Sgr A-F. The levels are from 200 to 1300 in steps of 100 Jy.kms^{-1}. The points are the observed positions, and the filled squares, the compact HII regions (positions from Ekers et al. 1983).

in our beam and an overall distribution offset from the compact H II regions (Fig. 4). In Sgr A-A, there is also a very broad (15 to 20 kms^{-1} wide) underlying component centered at about 45 – 50 kms^{-1}, which is still quite strong (30 to 40 Jy). This component shows a trend towards smaller velocity ($\approx$ 37 kms^{-1}) in the south. In Sgr A-F, the broad velocity component is centered at 20 kms^{-1}. The overall distribution of the emission in Sgr A-A shown in Fig. 4 is quite similar to the distribution observed in other molecules: the J=5–4 and J=7–6 lines of CS (Serabyn et al. 1992) and the J=2–1 line of ^{13}CO (Zylka et al. 1990). The similarity with the NH_3 distribution is less clear: the southern peak coincides with the weaker peak in the NH_3(2,2) map of Okumura et al. (1989) but their northern maximum seems to lie between our northern and southern peaks.

The methanol emission in Sgr A-G is much weaker, with 2 components of width 2.5 to 3 kms^{-1}, superimposed on broader features. There are no spikes, i.e. strong components of width narrower than 1.5 kms^{-1}, so we did not extend the map. This region was previously completely mapped with a larger beam by Szczepansky et al. (1989) in the 36 GHz transition.

3.3. The Orion region

3.3.1. OMC1

We have mapped the methanol emission in the region from IRc2 to the southern source S6 (Batrla et al. 1983), with 10″ spacing. The overall distribution of the emission (Fig. 6) is similar to that observed by Menten et al. (1988a) in the $5_{-1} \rightarrow 4_0$E transition at 84 GHz. There is an $\sim$ 30″ emission region south of IRc2, and another emission region centered slightly south of S6. No emission was detected between these two sources (unlike in CS and C^{18}O). For the emission south of IRc2, the line shape is quite different, narrower (but with no high velocity wings) and with two spikes not seen in the $5_{-1} \rightarrow 4_0$E transition (Fig. 5). These two spikes may correspond to some of the 25 GHz methanol masers detected at about the same position and velocity (features number 13 to 16 of Johnston et al. (1992)), although our much lower resolution than the resolution of these observations makes a precise identification difficult. We did not detect any narrow feature corresponding to the 8.6 kms^{-1} maser detected in the $7_0 \rightarrow 6_1 A^+$ transition at 44 GHz (Haschick et al. 1990).

Our map does not include the entire S6 position. For the region south of IRc2, we did not detect the wings observed in the 84.5 and 96.7 GHz methanol transitions; we do find a narrower feature superimposed on the most prominent 3 kms^{-1} wide feature. Presumably this narrow feature is produced by maser emission.

3.3.2. OMC2

OMC2 is one of the strongest methanol maser source detected at 44 GHz (peak intensity of more than 240 Jy, see Haschick et al. 1990), with a remarkable similarity of line shape in the different methanol maser transitions detected at 25, 36, 84 and 95 GHz, (Menten, 1991a). In our 15″ spacing map, the 36 GHz maser seems to lie about 10″ north to the position of the 25 GHz masers (Menten et al. 1988b). This is coincident with the position of IRS4, but the difference could also be due to pointing errors (see Sect. 2).

3.4. The W51 region

We have made 9 point maps with 15″ spacing around the positions MM1 to MM5 where methanol masers were detected in the 25 GHz transitions (Menten et al. 1986) and subsequently in the $7_0 \rightarrow 6_1 A^+$ transition at 44 GHz (Haschick et al. 1990) and also around the compact H II region e1/e2. Unlike Sgr B2, we find no very strong broad emission in this region. Rather there is only broad quasi-thermal emission toward W51e1/e2, W51-MM3 and W51-MM5. On this emission are superposed a group of narrow ($\leq$ 0.5 kms^{-1}) features (see Fig. 7); these appear near but not exactly at the same position and velocity as features detected in the 25 and 44 GHz transitions. Toward the W51-MM1 position, no emission was detected; the 54 kms^{-1} feature detected in the 25 GHz transition is located to the north-east, in a position corresponding more to the MM3 position, as

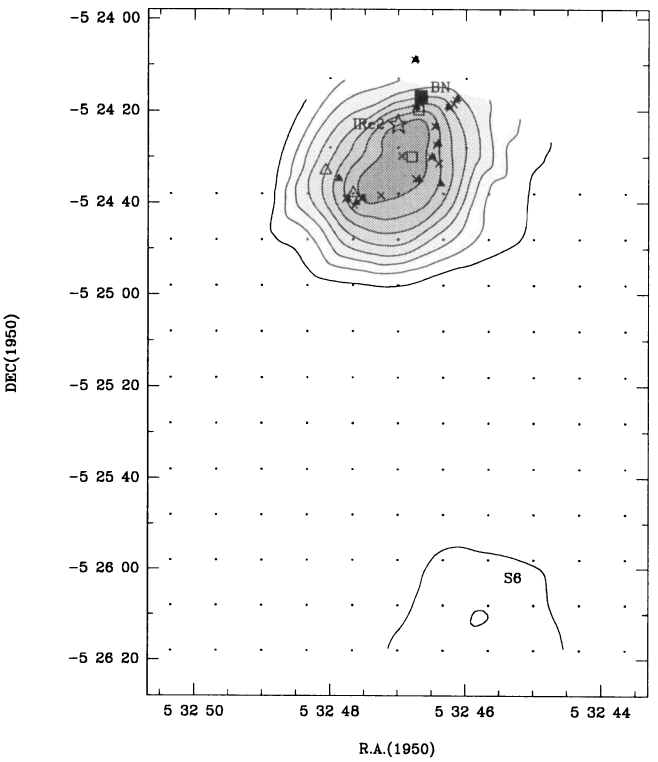

Fig. 6. Contour map of the 36 GHz methanol integrated intensity in Orion (OMC1) over the 0–15 kms^{-1} velocity range. The levels are from 5 to 50 in steps of 5 Jy.kms^{-1}. The points are the observed positions, the star is IRc2 and the filled square is the BN object. The unfilled triangle are the 36 GHz methanol masers (this paper), and the unfilled squares, the 95 GHz methanol masers (Plambeck and Wright 1988). Finally, the small crosses and filled triangles are the 25 GHz masers, respectively the $6_2 \rightarrow 6_1$E and the $5_2 \rightarrow 5_1$E transitions (Johnston et al. 1992).The S6 NH_3 condensation (Batrla et al. 1983) is also indicated.

it was observed in the 44 GHz transition. Toward the MM3 position, we did not detect the 59.3 kms^{-1} narrow feature detected at 25 GHz (but not at 44 GHz). Toward W51e1/e2, we detected no counterpart to the 49 kms^{-1} strong narrow feature observed at 44 GHz, but a narrow feature at 52.9 kms^{-1}, which was not previously observed.

3.5. The DR21/W75 region

This region, located in the Cygnus X complex, has been mapped with high resolution in different molecular transitions (see e.g. Wilson & Mauersberger, 1990). Together with Orion-KL, DR21(OH) is the only Class I methanol maser source with interferometrically determined maser positions (Batrla & Menten, 1988; Plambeck & Menten, 1990). In this region we have mapped those sources for which methanol masers were detected in other transitions.

3.5.1. DR21(OH)

The methanol maser emission in the OH maser/far-infrared source DR21(OH)/W75 S was mapped with high resolution in the $5_{-1} \rightarrow 4_0$E transition at 84 GHz by Batrla & Menten (1988; hereafter BM88) and in the $8_0 \rightarrow 7_1A^+$ transition at 95 GHz by Plambeck & Menten (1990). We have mapped 5×5 points with $12''$ spacings centered at the strongest methanol maser position. We extended this map to the south-east to cover the southern emission detected by BM88 (sources 5 and 6). An additional 5×6 point map with $20''$ spacings and 60 seconds integration time per position was made in February 1994. The positions and distribution of the 36 GHz emission are remarkably similar to what was observed by BM88 (see the two spectra in Fig. 8 and the spectra 2 and 5 in Fig. 2 of BM88). The velocities are also the same, taking into account that the rest frequency of the $5_{-1} \rightarrow 4_0$E transition used in BM88 is slightly higher than the more accurate value calculated later by De Lucia et al. (1989). The only clear difference is the non-detection of the -6.4 kms^{-1} feature toward the position 4 of BM88. The -0.5 kms^{-1} feature towards position 2 of BM88 is blended with the broader (thermal) underlying emission and is clearly present in only one of our spectra (it is not recorded in Table 1). The same is true for the -4.7 kms^{-1} features towards position 3 of BM88 and the -5.4 kms^{-1} features in the south, which are blended with our broad extended component at -3.6 kms^{-1}. This latter feature has the same central velocity and line width and peaks at the same position as the CO5 peak observed in $C^{18}O$(2–1) by Wilson & Mauersberger (1990) and seems clearly to be thermal emission.

3.5.2. DR21-MM

DR21-MM, also called DR21-West or DR21-W is a strong methanol maser source located about $75''$ west of the DR21 continuum source (a cluster of compact H II regions), in the western lobe of the prominent outflow detected in $C^{18}O$ by Wilson & Mauersberger (1990). Maser emission at -2.6 kms^{-1} was first detected in the 25 GHz transitions by Menten et al. (1986) and subsequently in the 36, 44, 84 and 95 GHz transitions (see e.g. Menten, 1991a) Another feature at -3.7 kms^{-1} was detected close to the DR21 continuum source in the $7_0 \rightarrow 6_1A^+$ transition by Bachiller et al. (1990), and subsequently in the $8_0 \rightarrow 7_1A^+$ transition at 95 GHz (Plambeck & Menten, 1990). We mapped the 36 GHz line around the DR21-MM position and extended our map eastward to the DR21 continuum source. We confirm the previous observations: there is a strong narrow feature at -2.7 kms^{-1} towards DR21-MM, but no other feature in a 1.5 arcminute region to the east. Moroever, unlike the line detected at 44, 84 and 95 GHz, towards DR21-MM no "pedestal" feature appears at 36 GHz at a 0.5 Jy level (see Fig. 8).

3.5.3. W75S(3)

W75S(3) is a water maser source in the northern part of the DR21/W75S region. The strongest methanol emission of the whole DR21/W75 region was detected towards this source at a

velocity $v_{LSR} = 0\,kms^{-1}$ (see Fig. 8). A narrow feature at this velocity was also detected at 44 GHz (Bachiller et al. 1990), but weaker than the two other features, at -5.2 and $-3.4\,kms^{-1}$. For these, we have detected a counterpart at 36 GHz. The strong feature at $v_{LSR} = 0\,kms^{-1}$ is not centered at the position of the W75S(3) water maser but at a position which corresponds roughly to the CS 10/NH_3 5 peak position of Wilson & Mauersberger (1990). This strong feature shows a red wing and can be decomposed in 2 gaussians, a strong, narrow point-like feature at $v_{LSR} = -0.17\,kms^{-1}$ and a weaker, broader and more extended feature at $v_{LSR} = 0.3\,kms^{-1}$.

3.5.4. W75N

W75N is another water vapor maser source located about 15′ north of W75S. Methanol maser emission was detected 22″ north from this source at 44 GHz (Haschick et al. 1989), but Haschick & Baan (1989) detected only a broad weak feature (probably quasi-thermal emission) at 36 GHz. We observed a 5×5 point map with with 20″ spacings around the W75N position, and we have detected a weak narrow ($0.6\,kms^{-1}$) feature at $10.0\,kms^{-1}$, 20″ east of the water maser source, superimposed on a broader, more extended feature.

3.6. G5.89–0.39

G5.89–0.39, also named W28 A2, is an ultra-compact H II region (Wood & Churchwell 1989) associated with OH and H_2O masers and with one of the most energetic high velocity bipolar outflow (Harvey & Forveille 1988; Choi et al. 1993). Two narrow methanol maser features at 8.8 and $12.2\,kms^{-1}$ have been detected by Bachiller et al. (1990) in the $7_0 \rightarrow 6_1A^+$ transition. Our 10″ resolution map around the water maser source W28 A2(1) (Genzel & Downes, 1977) show that up to five narrow velocity features can be distinguished in the $4_{-1} \rightarrow 3_0$E transition (Fig. 9), distributed in two groups: one at 8–9 kms^{-1} on the center and east and one at 11.5–12.5 kms^{-1} on the west. Unpublished data taken with the IRAM 30-meter telescope show a similar distribution in the $8_0 \rightarrow 7_1A^+$ and $9_0 \rightarrow 8_1A^+$ methanol transitions. There is not a one-to-one correspondence between the masering features, only 3 narrow features were detected in these transitions. Apart from the broadest component at $8.4\,kms^{-1}$ centered on the water maser position, the observed methanol emission does not correlate well with the ammonia emission (Gómez et al. 1991; Wood 1993) which is oriented north-east south-west nor with the infrared sources (Oliva & Moorwood 1986; Harvey et al. 1994), and the four methanol maser features at 8.3, 9.0, 11.5 and $12.2\,kms^{-1}$ seem to lie on the edges of the high velocity CO outflow (Choi at al. 1993). The resolution of the CS maps of Cesaroni et al. (1991) is not high enough to allow a precise comparison but the emission clearly extends to the west in the direction of the two higher velocity methanol masers. These appear to lie on the edge of the $C^{34}S$ emission.

3.7. G10.6–0.4

G10.6–0.4 (also known as G10.62–0.38, W31(2) or W31 C) is a well studied ultra-compact H II region where two methanol masers components at -6 and $-8\,kms^{-1}$ were detected by Menten et al. (1986) at 25 GHz about 10″ Northeast from the continuum source. The $-6\,kms^{-1}$ component has been also detected at 36 GHz (Haschick & Baan 1989) and at 44 GHz, a narrow feature appears at $-7\,kms^{-1}$ (Haschick at al. 1990). With our better spectral resolution (Fig. 9), we have separated the strong narrow feature into two narrower components. These seem to arise from the same position to within our accuracy. In addition we have detected another possible narrow feature 15″ northwest of the continuum source at $-2\,kms^{-1}$. The underlying broad emission is more or less centered on the continuum source and elongated in the southwest–northeast direction, that is, in the opposite direction of the flattened rotating core seen in other molecules such as $C^{18}O$ and NH_3 and CS (Ho et al. 1994; Guilloteau et al. 1988; Omodaka et al. 1992; see also Cesaroni et al. 1991). But as in these other molecules, we can see a marked velocity gradient of the broad emission from Southeast to Northwest.

3.8. W33

We have mapped the $4_{-1} \rightarrow 3_0$E methanol transition with 12″ spacing around the methanol maser discovered by Menten et al. (1986) in the $6_2 \rightarrow 6_1$E transition at 25 GHz, and subsequently detected in the $7_0 \rightarrow 6_1A^+$ transition at 44 GHz (Haschick et al. 1990) about 40″ west of the W33–Main H II region. Our $32.5\,kms^{-1}$ narrow feature (see Fig. 9) is at about the same position and velocity as the 25 GHz maser and the strongest feature found in the 44 GHz transition. We have also clearly detected two other narrow features: one in the south-west at $35.9\,kms^{-1}$ which might correspond to the 44 GHz higher velocity feature and another at lower velocity 27″ east. We have also detected a broad underlying component. The position is less certain, but seems to peak at the position of the compact core of the H II region (see e.g. Ho at al. 1986).

A comparison with the NH_3 maps of Keto & Ho (1989) seems to show that the methanol masers are coincident with the western ammonia shell, between the aligned northeast–southwest clumps at the corresponding velocity. This is the case for the 32.5 and $35.9\,kms^{-1}$ features.

3.9. NGC 7538

NGC 7538 is an active star forming region in the Perseus arm, with several H II regions, infrared sources, masers (OH, H_2O, NH_3, CH_3OH) and high velocity flows within a few arcminutes (see e.g. Kameya et al. 1989). Class II methanol masers have been detected near the ultra-compact H II region associated with the infrared source IRS1 (Batrla et al. 1987; Menten, 1991b), and a Class I methanol maser has been detected in the $7_0 \rightarrow 6_1A^+$ transition at 44 GHz about 40″ Southeast of IRS1 (Bachiller et al. 1990). Broad emission was also reported in this transition and in the $4_{-1} \rightarrow 3_0$E 36 GHz transition towards

NGC 7538(S), a region about 80″ south of IRS1, associated with the southern OH and H_2O masers and the infrared source IRS11 (Haschick et al. 1990; Haschick & Baan 1989). In October 1992, we made two 3 × 3 point maps with 15″ spacing around IRS1 and NGC 7538(S). Unlike Haschick & Baan (1989), we did not detect any emission towards IRS1. Since the strongest emission seemed to arise from the southwest, we have extended the map in March 1993 in this direction and in the south to connect with the map around NGC 7538(S). The emission detected southwest of IRS1 is quite complex with many narrow features (only the definite detections are in Table 1, but other possible narrow features are present at our detection limit level) superimposed on a broader component. The broad emission is somewhat extended and the peak seems to coincide with one of the CS clumps, CS4, detected by Kawabe et al. (1992) outside the CS ring-like structure around IRS1. This clump also appears in HCN and HCO^+ (Batrla et al. 1988; Pratap et al. 1990). The strongest narrow features are located southwest of the broad emission, and are more probably associated with the IRS11 outflow, since they lie only few arcsecond north of its blue lobe (Kameya et al. 1989). There is no direct association with the OH and H_2O masers of the region. One can also note that the strong (several tens of jansky) 57.4 kms^{-1} feature detected at 44 GHz southeast of IRS1 does not seem to have a counterpart at 36 GHz, since, although we have not extended the map southeast of IRS1 more than up to the offset (15″,−15″), such strong feature should have shown up at this position (but the line detected by Haschick & Baan (1989) towards IRS1 is much stronger that ours).

Towards NGC 7538(S), we have detected a strong broad emission from which some possible narrow features cannot be clearly distinguished. The emission peaks between IRS11 and the red lobe of its associated outflow (Kameya et al. 1989).

3.10. NGC 2071

We have mapped the $4_{-1} \rightarrow 3_0$E methanol transition with 15″ spacing around the center of the NGC 2071 bipolar outflow, one of the best studied high velocity molecular outflows. Methanol maser emission has already been detected in this transition (Haschick & Baan 1989), but no emission was detected in the $7_0 \rightarrow 6_1A^+$ transition at 44 GHz (Haschick et al. 1990). Our better resolution allows us to further resolve the features detected by Haschick & Baan (1989) into narrower components (Fig. 10 and Table 1). All the four narrow features as well as the broad underlying emission are located in a region ∼ 20″ south of the three infrared sources (IRS1, IRS2 and IRS3) detected at 10μm (Persson et al. 1981), and the peak of the shocked H_2 and CS emission (Kitamura et al. 1992). The methanol masers also do not coincide with the H_2O and OH masers nor with any of the CO clumps, which are located ∼ 10″ east of the most prominent redshifted clump (Moriarty-Schieven et al. 1989).

3.11. NGC 2264

We have mapped the $4_{-1} \rightarrow 3_0$E methanol transition with 12″ spacing around the bright infrared source IRS1 in the young cluster NGC 2264. A strong Class I methanol maser has been detected few seconds west of this source in many transitions (Menten 1991a; Haschick et al. 1990). Our better spectral resolution allows us to clearly separate the two narrow features seen in the 44 GHz line (Haschick et al. 1990) and blended in the spectrum at 36 GHz of Haschick & Baan (1989). The map confirms that the position of the maser is ∼ 10″ west of IRS1, with a distance of ∼ 5″ between the two narrow features. The broad underlying component extends outside the limit of our map north and east of IRS1. This is also the direction of the molecular cloud peak positions (see e.g. Crutcher et al. 1978; Krügel et al 1987).

3.12. G8.67–0.36

We have made 5×5 points map with 15″ spacing around G8.67–0.36, a core-halo type ultra-compact H II region (Wood & Churchwell 1989). We have detected several narrow features superimposed on a broad underlying component (Fig. 10), a line shape very similar to one observed in the $7_0 \rightarrow 6_1A^+$ transition at 44 GHz (Haschick et al. 1990), taking into account the better spectral and spatial resolution. The narrow features are located about 10″ north from the continuum source, on the opposite direction of the water maser located 6″ south (Dinger & Dickinson 1980). It should be noted that the velocity of the 36 and 44 GHz methanol emission is outside of the velocity range of the Class II methanol masers detected in this source (40–46 kms^{-1}, see Koo et al. 1988).

3.13. G30.8–0.1

We have mapped the G30.8–0.1 H II region within the W43 complex with 15″ spacing, around the water maser source on the eastern edge of the region W43 Main(3) where methanol maser emission has been detected in the $7_0 \rightarrow 6_1A^+$ transition (Haschick et al. 1990). Our better spectral and spatial resolution allow us to detect narrow velocity features superimposed on the broad line, which were not clearly seen in the spectrum of Haschick & Baan (1989). The strongest narrow feature is located about 17″ north of the water maser position. No feature appears to be coincident with the infrared and continuum sources (see Lester et al. 1985).

4. Discussion

4.1. Emission characteristics

As previously noted, the high spectral and spatial resolution and sensitivity of the survey allows us to detect many more narrow components than in the previous survey of Haschick & Baan (1989). However although we have not detected the weak broad components in all cases found by Haschick & Baan (1989). This emission is probably too extended, with a low source brightness in sources such as W48, W51N and G43.8–0.1. In fact, the detection of a single feature is rather exceptional. Only three sources, OMC2, G35.05–05 and DR21-MM definitely show one single narrow feature characteristic of maser emission; three more,

S235B, W75N and G34.3+0.2 show one single narrow feature superimposed on a broad underlying component (Fig. 8 and 11). For most of the sources where strong emission was detected, the situation is more complex, with several narrow features, which are usually not spatially coincident, superimposed on a wider plateau-like feature, probably of quasi-thermal origin. The most extreme cases are the galactic center sources Sgr A and Sgr B2, where several tens of features, both narrow and broad, can be distinguished (see Fig. 1, 3, 5 and 7 to 11).

Can the narrow ($\leq 1.5\,\mathrm{kms}^{-1}$) features always be identified as maser emission and the broad ($\geq 2\,\mathrm{kms}^{-1}$) features as quasi-thermal emission? Although the narrow features are not always very strong, these have linewidths which are usually much smaller than for the other molecules (and also smaller than an underlying component). Since these arise from a region point-like in our beam, their brightness temperature is usually too high to be consistent with thermal emission. However, for the weaker sources, interferometric measurements are needed to confirm maser emission. The only clear exceptions are probably the sources observed in the ρ Oph region (ρ Oph and the source named ROPHS1 in our survey) where the narrow line width observed ($0.8\,\mathrm{kms}^{-1}$) is also typical for the other molecules, and the emission is clearly extended; this indicates that the brightness temperatures are sufficiently low to be consistent with thermal emission.

For the broad components, the line width is usually typical for the molecules of the region, and the emission is often extended. This is similar to the emission observed in other high density molecular tracers. This suggests that normal, quasi-thermal emission from the molecular clouds is the excitation process. Particularly exceptional cases are the quite broad ($\approx$ 3 or $4\,\mathrm{kms}^{-1}$ wide) strong components detected around Sgr B2 and Sgr A. These are point-like, and so have a derived brightness temperature from 300 to 700 K, which is higher than the highest proposed temperature for the region. This can only be explained by maser emission. The broad component of G30.8–0.1 could also be a maser of the same kind since its derived brightness temperature, 120 K, is higher than the kinetic temperature of the region (40 to 70 K) proposed by Lester et al. (1985).

4.2. Comparison with other methanol maser transitions

Our results confirm also the tendency of the methanol maser in the 25, 36, 44, 84 and 95 GHz transitions (Class I methanol masers) to arise from the same regions: we have discovered maser emission at 36 GHz in a number of sources where 44 GHz maser emission has been previously detected (S231, G5.89–0.39, G8.67–0.36, W33, W42, G35.05–0.5, W75S(3)), and for many sources, the line shape and features are similar. However, the emission at 36 GHz is usually less intense than at 44 GHz one. The emission seems to be spatially coincident, when maps are available (e.g. DR21(OH) at 84 and 95 GHz, G5.89–0.39 at 95 GHz). But there are some cases where the emission in the different Class I methanol maser transitions is quite different. The best examples are the galactic center sources Sgr B2 and Sgr A-A, but there are also notable differences in some sources. For W51 E1, the $49\,\mathrm{kms}^{-1}$ feature observed at 44 GHz is not present at 36 GHz, for W75S(3), the $0.3\,\mathrm{kms}^{-1}$ feature observed at 36 and 44 GHz is not present at 95 GHz, for DR21, the $-3.7\,\mathrm{kms}^{-1}$ feature observed at 44 and 95 GHz is not present at 36 GHz, for NGC 7538, the strong $57.4\,\mathrm{kms}^{-1}$ feature observed at 44 GHz is not present at 36 GHz, and for Orion no narrow emission features are detected at 84 GHz. This suggests that although these different transitions usually need the same excitation conditions to produce maser emission, there are cases for which the conditions are valid for one transition but not for other. In the next section, we show the results of detailed statistical equilibrium calculations which could explain the observations.

The relation with Class II (12.2 and 6.6 GHz transitions) masers is more indirect. Class II methanol masers have been indeed detected in some Class I methanol maser sources (Menten, 1991b) but the line profile observed in the two classes are very different. In this case, interferometric measurements have shown that the Class II methanol masers are closely associated with the H II regions. The coincidence of both methanol maser classes is thus probably only apparent, caused by the large beamwidths of the observations.

4.3. Excitation and statistical equilibrium calculation

As noted by several authors (see e.g. Menten, 1991a), collisional excitation leads naturally to the inversion of the $4_{-1} \rightarrow 3_0$E methanol transition, from the basic properties of the molecule. The reasons are: (1) the $k = -1$ ladder of the E torsional species is the end point for spontaneous decay from the neighbouring ladders, (2) collisions favor $\Delta k = 0$ transitions, so that the lower levels of the $k = -1$ ladder are rapidly populated, leading to overpopulation of these levels with respect to the $k = 0$ level. Therefore, maser action is expected in the $4_{-1} \rightarrow 3_0 E$ transition at 36 GHz, in the $5_{-1} \rightarrow 4_0 E$ transition at 84 GHz and in the $6_{-1} \rightarrow 5_0 E$ transition at 132 GHz. For the A-symmetry species, the same situation occurs for the $k = 0$ ladder, and so, maser action is expected in the $7_0 \rightarrow 6_1 \mathrm{A}^+$, the $8_0 \rightarrow 7_1 \mathrm{A}^+$ and the $9_0 \rightarrow 8_1 \mathrm{A}^+$ transitions at 44, 95 and 146 GHz respectively. However, this simple mechanism cannot explain the $J_2 - J_1$ masers at 25 GHz. For these masers, Johnston et al (1992) have used the ad hoc assumption of preferred $|\Delta k| = 3$ collisional transitions (at rate 10% of the $\Delta k = 0$ rate) and forbidden $|\Delta k| = 2$ transitions.

In order to better determine the physical conditions which give rise to the Class I methanol maser emission, we have performed statistical equilibrium calculations for various temperatures, densities and methanol abundances. using a statistical equilibrium program. This program includes the 100 lowest energy levels for either the E or A symmetry species (up to 144 K above the ground state for the E species and up to 154 K above the ground state for the A species). Details of the program can be found in Walmsley et al. (1988) and Johnston et al. (1992). We have only considered the $\Delta k = 0$ and $|\Delta k| = 1$ collisional transitions and assumed that collisional transitions for the other Δk's are forbidden. Then, this model cannot produce 25 GHz methanol masers. Fig. 4.3 shows the results for

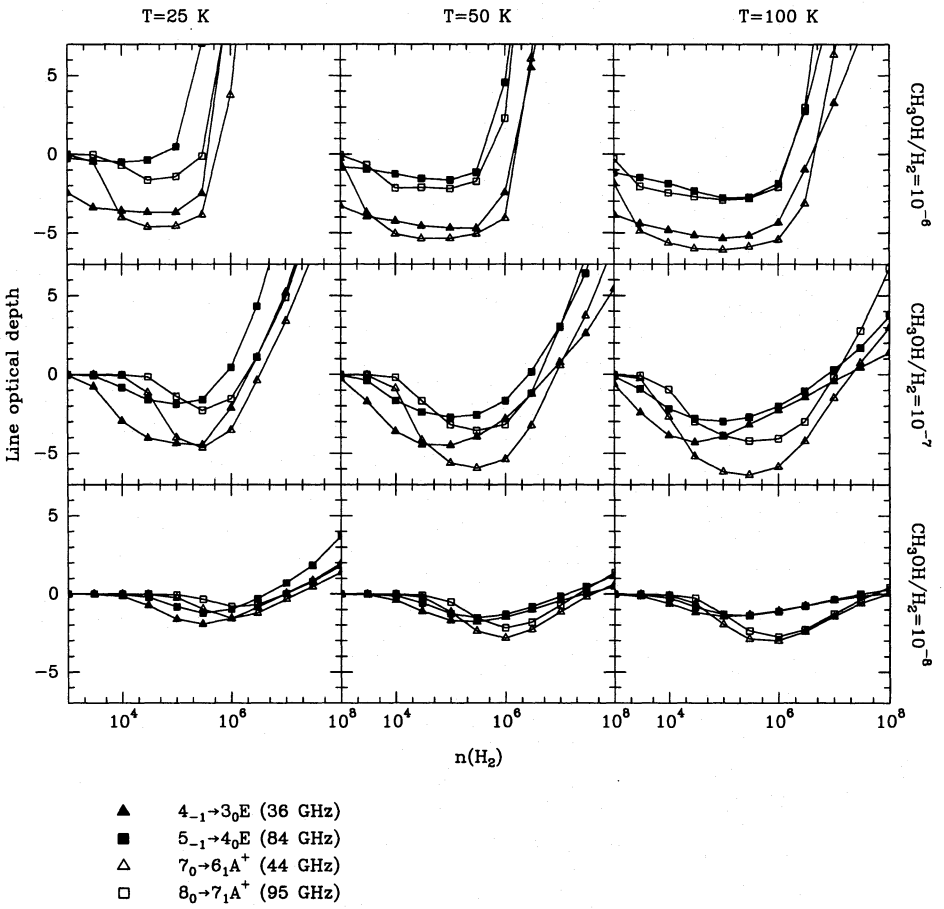

Fig. 12. Line optical depth of the $4_{-1} \rightarrow 3_0$E (filled triangles), the $5_{-1} \rightarrow 4_0$E (filled squares), the $7_0 \rightarrow 6_1$A$^+$ (unfilled triangles) and the $8_0 \rightarrow 7_1$A$^+$ (unfilled squares) methanol transitions in function of the hydrogen density for various temperatures and methanol abundances.

the 36, 44, 84 and 95 GHz maser transitions for temperatures from 25 to 100 K, methanol abundances from 10^{-8} to 10^{-6} and hydrogen densities from 10^3 to 10^8 cm^{-3}. We can see that at low methanol abundance the line optical depths are similar for the transitions of the same species, that is for the 36 and 84 GHz transition on the one hand and for the 44 and 95 GHz on the other. But at high methanol abundances the line optical depth is similar for the transitions in the same frequency range (except for $n(H_2) \leq 10^4$). At intermediate methanol abundances, the situation is mixed; however, one notes that in the same methanol species, the line optical depth is always lower for the lower frequency transition, whatever the physical conditions. This remark is also valid for the higher frequency transitions $6_{-1} \rightarrow 5_0$E and $9_0 \rightarrow 8_1$A$^+$ at 132 and 146 GHz, which have an higher optical depth than respectively the $5_{-1} \rightarrow 4_0$E and $8_0 \rightarrow 7_1$A$^+$ transitions at 84 and 95 GHz. The effect of increasing kinetic temperature increases the density range for which maser action occurs.

All cases where simultaneous maser action occurs at 36, 44, 84 and 95 GHz can be explained by this simple model. However, it is probable that the external radiation field of H II region or of internal dust plays an important role for some of the observed sources in our sample.

4.4. Location of the emission

Our observations confirm, for a wider sample, the previous results from selected regions that the Class I methanol masers are usually found offset from the compact H II regions, infrared sources, OH and H_2O masers, that is the usual indicators of newly formed stars, often by more than 15–20″. This is striking for the ultra-compact H II regions (UCHII): among the 10 sources of the survey of Wood & Churchwell (1989) that we have observed (G5.89–0.39, G8.67–0.36, G10.30–0.15, G10.6–0.4, G11.94–0.62, G29.96–0.2, G34.3+0.2, g35.05–0.5, ON2 and NGC7538-IRS1), a narrow feature typical of maser emission was detected within 5″ radius of the UCHII only in one source G5.89–0.39; this is a special case, since the maser is associated with very energetic high velocity bipolar outflow (and the other narrow features are located further away, see our discussion for this source). All other masers found near these regions (7 sources) have larger offsets from the continuum emission peaks. The other exception is the coincidence of the methanol maser in OMC2 with the infrared source IRS4 (but higher resolution observations are needed to confirm this coincidence). Such coincidences might also be a simple line of sight effect.

In the molecular outflow sources (G5.89–0.39, NGC 2071, DR21-MM, NGC 7538) the methanol masers are often located at the edges of the outflow lobes as traced by other molecules

such as CO. This reinforces the suggestion of Plambeck & Menten (1990), that the interaction of outflow with dense clumps of gas lead to the formation of methanol masers, by enhancing the abundance via release of methanol from grains surfaces, due to the shock heating. Statistical equilibrium calculations (Menten 1991a), show indeed that high (10^{-7}) methanol abundance is needed to produce maser emission in the Class I transitions. This could also explain why thermal methanol emission is often associated with the maser emission. But it should be noted that the maser features are generally *not* coincident with the thermal methanol emission peaks, which are more closely associated with the observed emission peak in other molecules, especially with the high density tracers such as CS. However, intense maser emission also requires small velocity gradients or turbulence along the line of sight to allow the line intensity to build up. Clearly, more high resolution observations of such sources are needed to confirm these results, and determine the characteristics of the clump where the methanol maser emission arise.

5. Conclusions

The high spatial and spectral resolution of our survey of the $4_{-1} \rightarrow 3_0$E methanol transition shows that narrow emission features typical of maser emission are much more frequent than previously observed: we have found such narrow features in 28 sources among the 48 surveyed. And in 20 sources, we have detected several narrow features. In most sources, these narrow features are superimposed on a broad underlying component. We indentify the narrow features with high intensity masers, and the broader features with quasi-thermal emission or perhaps low intensity masers.

The high intensity masers are generally found at least several arcseconds offset from the usual newly formed star indicators (compact H II regions, infrared sources, water and OH masers), and also from the peak of molecular emission, as observed in CO and/or CS, as well as hot molecular cores. However, there is a good correlation with the other Class I methanol masers observed at 25, 44, 84 and 95 GHz, often (but not always) with an exact correspondence (in velocity and position) of the features. This suggests that the conditions needed to produce to Class I methanol maser emission are nearly the same for the different Class I transitions. This observational result is consistent with the statistical equilibrium calculations.

Finally it can also be noted, that, as in previous observations, no variability of the 36 GHz methanol emission could be observed between our October 1992, March 1993 and February 1994 observing sessions (16 sources were observed during two sessions and one source, DR21(OH), during the three sessions).

Acknowledgements. We would like to thank C.M.Walmsley for providing the statistical equilibrium program used in Sect. 4.3 and for his helpful comments on the text, C.Codella for careful reading of the text and A.Tieftrunk and D.Balser for help during the observations. S.L. thanks the Max-Planck Institut für Radioastronomie and the Spanish DGICYT (grant number PB93-04) for their partial support during this work.

References

Bachiller, R., Menten, K.M., Gomez-Gonzalez, J., Barcia, A., 1990, A&A, 240, 116
Batrla, W., Wilson, T.L., Bastien, P., Ruf, K., 1983, A&A, 128, 279
Batrla, W., Matthews, H.E., Menten, K.M., Walmsley, C.M., 1987, Nature, 326, 49
Batrla, W., Menten, K.M., 1988, ApJ, 329, L117
Batrla, W., Pratap, P., Snyder, L.E., 1988, ApJ, 330, L67
Cesaroni, R., Walmsley, C.M., Kömpe, C., Churchwell, E., 1991, A&A, 252, 278
Choi, M., Evans, N.J.II, Jaffe, D.T., 1993, ApJ, 417, 624
Crutcher, R.M., Hartkopf, W.I., Giguere, P.T., 1978, ApJ, 226, 839
De Lucia, F.C., Herbst, E., Anderson, T., Helminger, P., 1989, J. Molec. Spectrosc., 134, 395
Dinger, A., Dickinson, D.F., 1980, AJ, 85, 1247
Ekers, R.D., van Gorkom, J.H., Schwarz, U.J., Goss, W.M., 1983, A&A, 122, 143
Gaume, R.A., Claussen, M.J., 1990, ApJ, 351, 538
Genzel, R., Downes, D., 1977, A&AS, 30, 145
Gómez, Y., Rodríguez, L.F., Garay, G., Moran, J.M., 1991, ApJ, 377, 519
Guilloteau, S., Forveille, T., Baudry, A., Despois, D., Goss, W.M., 1988, A&A, 202, 189
Harvey, P.M., Forveille, T., 1988, A&A, 197, L19
Harvey, P.M., Lester, D.F., Colomé, C., Smith, B., Monin, J-L., Vauglin, I., 1994, ApJ, 433, 187
Haschick, A.D., Baan, W.A., 1989, ApJ, 339, 949
Haschick, A.D., Menten, K.M., Baan, W.A., 1990, ApJ, 354, 556
Ho, P.T.P., Klein, R.I., Haschick, A.D.,1986, ApJ, 305, 714
Ho, P.T.P., Terebey, S., Turner, J.L., 1994, ApJ, 423, 320
Johnston, K.J., Gaume, R., Stolovy, S., Wilson, T.L., Walmsley, C.M., Menten, K.M., 1992, ApJ, 385, 232
Kameya, O., Hasegawa, T.I., Hirano, N., Takakubo, K., Seki, M., 1989, ApJ, 339, 222
Kawabe, R., Suzuki, M., Hirano, N., Akabane, K., Barsony, M., Najita, J.R., Kameya, O., Ishiguro, M., 1992, PASJ, 44, 435
Keto, E.R., Ho, P.T.P.., 1989, ApJ, 347, 349
Kitamura, Y., Kawabe, R. Ishiguro, M., 1992, PASJ, 44, 407
Koo, B.-C., Williams, D.R.W., Heiles, C., Backer, D.C., 1988, ApJ, 326, 931
Krügel, E., Güsten, R., Schulz, A., Thum, C., 1987, A&A, 185, 283
Lester, D.F., Dinerstein, H.L., Werner, M.W., Harvey, P.M., Evans, N.J.II, Brown, R.L., 1985, ApJ, 296, 565
Lis, D.C., Goldsmith, P.F., 1991, ApJ, 369, 157
Martin-Pintado, J., de Vicente, P., Wilson, T.L., Johnston, K.J., 1990, A&A, 236, 193
Menten, K.M., Walmsley, C.M., Henkel, C., Wilson, T.L., 1986, A&A, 157, 318
Menten, K.M., Walmsley, C.M., Henkel, C., Wilson, T.L., 1988a, A&A, 198, 253
Menten, K.M., Walmsley, C.M., Henkel, C., Wilson, T.L., 1988b, A&A, 198, 267
Menten, K.M., 1991a, in Skyline, Proceeding of the Third Haystack Observatory Meeting, p. 119, eds. A.D. Haschick and P.T.P. Ho (Astr. Soc. Pac.).
Menten, K.M., 1991b, ApJ, 380, L79
Moriarty-Schieven, G.H., Snell, R.L., Hughes, V.A., 1989, ApJ, 347, 358
Morimoto, M., Ohishi, M., Kanzawa, T., 1985, ApJ, 288, L11

Okumura, S.K., Ishiguro, M., Fomalont, E.B., Chikada, Y., Kasuga, T., Morita, K.-I., Kawabe, R., Kobayashi, H., Inoue, M., Hasegawa, T., 1989, in "The center of the Galaxy", Proceedings of the 136th symposium of the I.A.U., p. 371
Oliva, E., Moorwood, A.F.M., 1986, A&A, 164, 104
Omodaka, T., Kobayashi, H., Kitamura, Y., Nakano, M., Ishiguro, M., 1992, PASJ, 44, 447
Persson, S.E., Geballe, T.R., Simon, T., Lonsdale, C.J., Baas, F., 1981, ApJ, 251, L85
Plambeck, R.L., Menten, K.M., 1990, ApJ, 364, 555
Pratap, P., Batrla, W., Snyder, L.E., 1990, ApJ, 351, 530
Szczepansky, J.C., Ho, P.T.P., Haschick, A.D., Baan, W.A., 1989, in "The center of the Galaxy", Proceedings of the 136th symposium of the I.A.U., p. 383
Serabyn, E., Lay, J.H., Achtermann, J.M., 1992, ApJ, 395, 166
Walmsley, C.M., Batrla, W., Matthews, H.E., Menten, K.M., 1988, A&A, 197, 271
Wilson, T.L., Mauersberger, R., 1990, A&A, 239, 305
Wood, D.O.S., 1993, in ASP Conf. Ser. 35, "Massive Stars, Their Lives in the Interstellar Medium", ed. J.P. Casinelli & E. Churchwell (San Fransisco, ASP), p. 108
Wood, D.O.S., Churchwell,E., 1989 ApJS, 69, 831
Zylka, R., Mezger, P.G., Wink, J.E., 1990, A&A, 234, 133

This article was processed by the author using Springer-Verlag LaTeX A&A style file *L-AA* version 3.